One-dimensional Antiferromagnetic Cycloheptatrienyl Molybdenum and Tungsten Compounds†

Malcolm L. H. Green, Andrew Harrison, Philip Mountford and Dennis K. P. Ng
Inorganic Chemistry Laboratory, South Parks Road, Oxford OX1 3QR, UK

The 17-electron compounds $[M(\eta\text{-}C_7H_7)LX_2]$ (M = Mo, L = MeCN, X = I **1**; M = Mo, L = PMe_3, X = I **2**; M = W, L = MeCN, X = I **3**; M = W, L = PMe_3, X = I **4**; M = W, L = PMe_3, X = Br **5**) have been prepared. All exhibit antiferromagnetic interactions with temperatures at χ_{max} ranging from 12 to 17 K. The magnetic susceptibility data have been described by one-dimensional magnetic models. The crystal and molecular structures of $[Mo(\eta\text{-}C_7H_7)(MeCN)I_2]$ **1** have been determined, and confirm the one-dimensional structure.

One-dimensional magnetic systems continue to excite the interest of experimentalists and theorists. This is partly due to the fact that they provide simple models for more complex magnetic materials, and partly because certain physical phenomena are unique to low-dimensional magnets. Although classical inorganic co-ordination compounds with a linear chain structure are known and have been studied extensively,[1] organometallic compounds, in particular of the early transition metals, have received much less attention. During the course of exploration of η-cycloheptatrienyl-molybdenum[2a] and -tungsten chemistry,[2b] we found that the 17-electron compounds $[M(\eta\text{-}C_7H_7)LX_2]$ (M = Mo, L = MeCN, X = I **1**; M = Mo, L = PMe_3, X = I **2**; M = W, L = MeCN, X = I **3**; M = W, L = PMe_3, X = I **4**; M = W, L = PMe_3, X = Br **5**) behaved as one-dimensional antiferromagnets. Here we describe the preparation of and magnetic studies on these compounds together with the crystal and molecular structure of $[Mo(\eta^7\text{-}C_7H_7)(MeCN)I_2]$ **1**.

Results and Discussion

Preparation and Characterisation of $[M(\eta\text{-}C_7H_7)LX_2]$.—The compounds $[M(\eta\text{-}C_7H_7)(\eta^5\text{-}C_7H_9)]$ (M = Mo or W) have been described previously.[3] However their syntheses were inconvenient since they required the metal vapour synthesis technique. Here we report much improved one-pot syntheses. Reduction of $MoCl_5$ or WCl_6 with Na/Hg in the presence of cycloheptatriene produces $[M(\eta\text{-}C_7H_7)(\eta^5\text{-}C_7H_9)]$ (M = Mo or W) in gram quantities. These compounds provide a direct entry to other cycloheptatrienyl-molybdenum or -tungsten complexes. Thus, their oxidation with iodine in acetonitrile gives purple crystals of $[Mo(\eta\text{-}C_7H_7)(MeCN)I_2]$ **1** or dark red crystals of $[W(\eta\text{-}C_7H_7)(MeCN)I_2]$ **3**, respectively. The MeCN ligands in **1** and **3** are labile and are readily displaced by PMe_3 to give the compounds $[Mo(\eta\text{-}C_7H_7)(PMe_3)I_2]$ **2** or $[W(\eta\text{-}C_7H_7)(PMe_3)I_2]$ **4** as red crystals. Similarly, oxidation of $[W(\eta\text{-}C_7H_7)(\eta^5\text{-}C_7H_9)]$ with bromine in tetrahydrofuran (thf) followed by treatment with PMe_3 gives orange-brown crystals of $[W(\eta\text{-}C_7H_7)(PMe_3)Br_2]$ **5**. The compounds **1**–**5** have been characterised by infrared and mass spectroscopy and micro-analysis (Table 1).

It has been proposed that the $\eta\text{-}C_7H_7$ ligand requires three electrons from the metal centre in the formation of the metal–ligand bonds.[4] Hence, the compounds **1**–**5** can be considered to have the d^1 electronic configuration. The solution EPR spectra of these compounds provided evidence to support this proposal (see data in Table 2). Fig. 1 shows the EPR spectrum of $[Mo(\eta\text{-}C_7H_7)(MeCN)I_2]$ **1** in thf. This appears to be symmetrical and consists of a main signal centred at $g = 2.02$ with a linewidth of 22 G. There is also hyperfine splitting due to molybdenum isotopes (^{95}Mo and ^{97}Mo have spin $\frac{5}{2}$) with A_{iso} = 46 G. However, the spectrum of **2** in thf showed only a broad signal without any hyperfine splitting. The spectra of **3**–**5** in thf or CD_3CN each exhibited a broad signal and no hyperfine coupling to ^{183}W or ^{31}P was observed; lowering the temperature to 153 K caused only a slight sharpening of the signals.

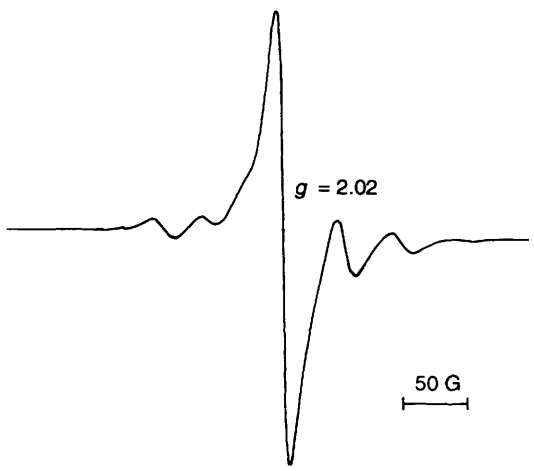

Fig. 1 The EPR spectrum of $[Mo(\eta\text{-}C_7H_7)(MeCN)I_2]$ **1** in thf at room temperature

Crystal and Molecular Structure of $[Mo(\eta\text{-}C_7H_7)(MeCN)I_2]$ **1**.—Single crystals of $[Mo(\eta\text{-}C_7H_7)(MeCN)I_2]$ **1** suitable for a crystal structure analysis were grown by cooling a concentrated acetonitrile solution. The molecular structure is shown in Fig. 2. It is a typical three-legged piano-stool type with the $\eta\text{-}C_7H_7$ ligand bonded symmetrically to the metal. The acetonitrile ligand is N-bonded to the Mo centre. Selected bond lengths and angles and the fractional atomic coordinates are given in Tables 3 and 4, respectively. These data are unexceptional.

Compound **1** crystallises in the triclinic crystal system with space group $P\bar{1}$. As shown in Fig. 3 the crystal structure consists of chains of molecules. The shortest intermolecular distance within a chain is 3.670 Å and occurs beteen I(1) and C(5) of the

† *Supplementary data available:* see Instructions for Authors, *J. Chem. Soc., Dalton Trans.*, 1993, Issue 1, pp. xxiii–xxviii.

Non-SI units employed: G = 10^{-4} T, emu = SI × $10^6/4\pi$.

Table 1 Analytical, infrared and mass spectroscopic data

Compound	Colour	Analysis[a] (%) C	H	Other	IR (cm^{-1}) and mass spectroscopic data[b]
1 [Mo(η-C_7H_7)(MeCN)I_2]	Purple	22.5 (22.4)	2.1 (2.1)	N 2.9 (2.9) I 53.1 (52.7)	ν(CN) 2270
2 [Mo(η-C_7H_7)(PMe_3)I_2]	Red	23.2 (23.2)	3.1 (3.1)	I 49.7 (49.1)	ν(PMe_3) 957 m/z[c] 519 (M^+), 443 (M − PMe_3)
3 [W(η-C_7H_7)(MeCN)I_2]	Dark red	18.7 (19.0)	1.8 (1.8)	N 2.5 (2.5) I 45.1 (44.5)	ν(CN) 2280, 2310 m/z[d] 570 (M^+)
4 [W(η-C_7H_7)(PMe_3)I_2]	Red	20.2 (19.9)	2.7 (2.7)	I 42.5 (42.0)	ν(PMe_3) 940, 956
5 [W(η-C_7H_7)(PMe_3)Br_2]	Orange-brown	23.9 (23.5)	3.1 (3.2)	Br 31.8 (31.3)	ν(PMe_3) 946, 962 m/z[d] 509 (M^+), 430 (M − Br)

[a] Calculated values given in parentheses. [b] The values for m/z are based on the most abundant isotope of each element. The bands show the predicted isotope-patterns. [c] By electron impact. [d] By fast atom bombardment.

Table 2 The EPR data for compounds **1**–**5**

Compound	g	Linewidth/G	Conditions
1*	2.02	22	In thf at 293 K
2	2.06	49	In thf at 293 K
3	1.941	56	In CD_3CN at 293 K
4	1.988	53	In thf at 153 K
5	1.943	57	In thf at 153 K

* A_{iso} 46 G.

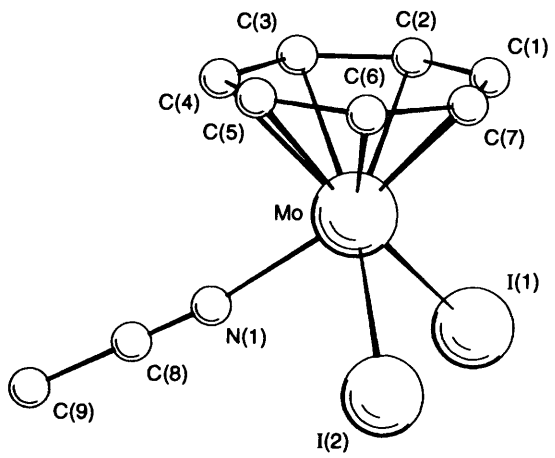

Fig. 2 Molecular structure of [Mo(η-C_7H_7)(MeCN)I_2] **1**. Hydrogen atoms omitted for clarity

Table 3 Selected bond lengths (Å) and angles (°) for [Mo(η-C_7H_7)(MeCN)I_2] **1**

Mo–I(1)	2.8210(4)	Mo–I(2)	2.8003(4)
Mo–N(1)	2.166(3)	Mo–C(1)	2.264(4)
Mo–C(2)	2.271(5)	Mo–C(3)	2.272(5)
Mo–C(4)	2.258(5)	Mo–C(5)	2.280(5)
Mo–C(6)	2.260(5)	Mo–C(7)	2.270(5)
N(1)–C(8)	1.135(6)	C(1)–C(2)	1.389(8)
C(1)–C(7)	1.389(9)	C(2)–C(3)	1.409(8)
C(3)–C(4)	1.392(9)	C(4)–C(5)	1.41(1)
C(5)–C(6)	1.42(1)	C(6)–C(7)	1.404(9)
C(8)–C(9)	1.450(6)	Mo–C_7(centroid)	1.592
I(2)–Mo–I(1)	87.47(1)	N(1)–Mo–I(1)	84.1(1)
N(1)–Mo–I(2)	84.6(1)	C(8)–N(1)–Mo	173.8(4)

Table 4 Fractional atomic coordinates for [Mo(η-C_7H_7)(MeCN)I_2] **1**

Atom	X/a	Y/b	Z/c
Mo	0.824 46(4)	0.361 01(5)	0.220 56(2)
I(1)	0.495 91(4)	0.040 65(5)	0.205 10(3)
I(2)	0.963 52(5)	0.197 35(6)	0.389 88(2)
N(1)	0.679 4(6)	0.521 4(6)	0.332 0(3)
C(1)	0.875 8(9)	0.230 6(9)	0.060 5(4)
C(2)	0.748 2(9)	0.359(1)	0.049 7(4)
C(3)	0.755 7(9)	0.560 7(9)	0.100 3(4)
C(4)	0.897(1)	0.681 1(8)	0.173 2(5)
C(5)	1.069 0(9)	0.635(1)	0.213 6(5)
C(6)	1.132 7(7)	0.449(1)	0.190 4(5)
C(7)	1.047 1(8)	0.268(1)	0.122 4(4)
C(8)	0.608 9(8)	0.621 1(7)	0.386 5(4)
C(9)	0.519(1)	0.752(1)	0.454 5(5)

η-C_7H_7 ring. This distance is shorter than the sum of the van der Waals radii of carbon and iodine (4.00 Å). The neighbouring chains are arranged antiparallel to each other as shown in Fig. 3(*a*) and 3(*d*). The distance between the centroids of cycloheptatrienyl rings of adjacent molecules is 3.710 Å, which is close to the interlayer distance of graphite (3.35 Å). In short, the structure may be described as a chain of dimers incorporated in a ladder-like arrangement while the pairs of molecules we call 'dimer' are depicted in Fig. 3(*a*) as A_2–B_1, A_3–B_2, *etc.*

Magnetic Properties of [M(η-C_7H_7)LX_2].—The molar magnetic susceptibility of [Mo(η-C_7H_7)(MeCN)I_2] **1** has been measured in the temperature range 2–300 K using a superconducting quantum-interference device (SQUID) magnetometer. The data are displayed in Fig. 4. The maximum at 16 K provides strong evidence for antiferromagnetic exchange interactions. The susceptibility falls to 0.15 χ_{max} at 3 K. On further cooling below 3 K the susceptibility rises, which may be due to the presence of traces of paramagnetic impurities or parasitic ferromagnetism. At higher temperatures (50–300 K) compound **1** obeys the Curie–Weiss law [$\chi_M = C/(T - \theta)$] with a Curie constant $C = 0.29$ emu K mol^{-1} and a Weiss constant $\theta = -5.2$ K. The negative Weiss constant suggests the presence of significant antiferromagnetic interactions. The effective magnetic moment μ_{eff} was calculated with the formula $\chi = N\mu_{eff}^2/3kT$ and the temperature dependence is shown in Fig. 5. At higher temperatures, μ_{eff} has a steady value of *ca.* 1.53 μ_B which is lower than the value of 1.75 calculated on the basis of the spin-only formula $\mu_{eff}^2 = g^2[S(S + 1)]$ where g is taken from the EPR data.

The compounds **2**–**5** have magnetic properties similar to those of **1** and the data are compiled in Table 5. However, for compounds **3** and **4**, the plots of $1/\chi_M$ *vs.* T were concave with small curvature at *ca.* 40–296 K. It was not possible to find a satisfactory least-squares fit of the data using the Curie–Weiss law. For each of the compounds **1**–**5** the moments were measured from 0 to 3 T at 6 K. Plots of magnetic moment against field gave straight lines which indicates that the

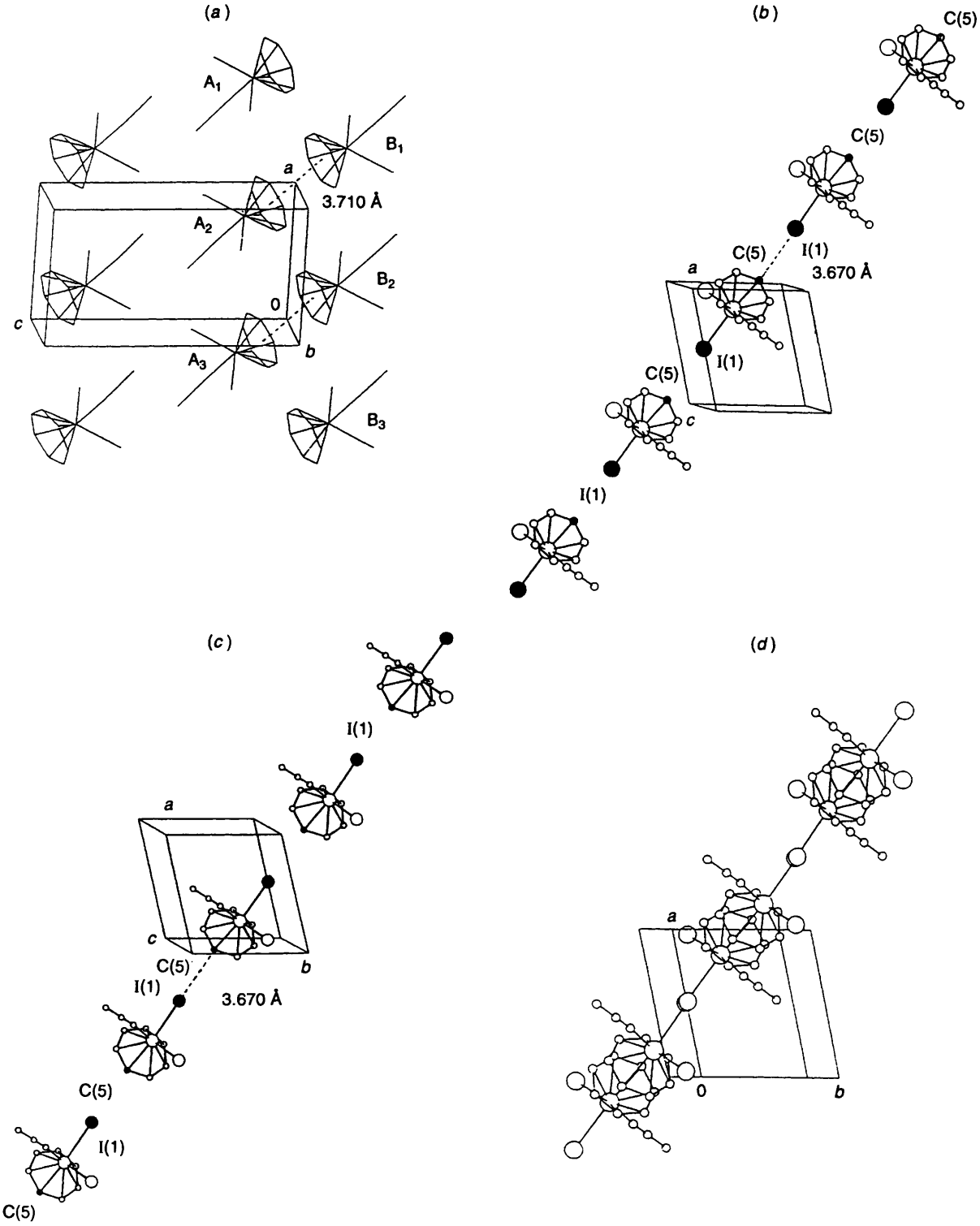

Fig. 3 Crystal structure of $[Mo(\eta\text{-}C_7H_7)(MeCN)I_2]$ **1**: (*a*) view along the *b* axis, (*b*) view of molecules A_x along the *c* axis, (*c*) view of molecules B_x along the *c* axis and (*d*) view along the *c* axis

magnetic data are field independent. For example, as shown in Table 5, changing the magnetic field from 0.2 to 1 T does not produce a significant change in the magnetic susceptibility data. The effective moment of these compounds depends on temperature in a similar manner to that for compound **1**. The steady values found at high temperatures are significantly lower than would be expected for a spin-only ion with $S = \frac{1}{2}$. We show the deviation from the predictions for spin-only ions in Table 5 in the form of values of g calculated using the spin-only formula and $S = \frac{1}{2}$. An analysis of the values of g from both the EPR and susceptibility data requires knowledge of the strength and symmetry of the ligand field and exchange interactions as well as an estimate of the covalency of the bonds between the metal and its ligands. In the absence of reliable estimates of all these quantities it is pointless to take the analysis further.

In the light of the structure of $[Mo(\eta\text{-}C_7H_7)(MeCN)I_2]$ **1**, we envisage that magnetic interactions may occur along the chains of iodide-bridged molybdenum centres through the superexchange mechanism. Interactions within the dimers of molecules [Fig. 3(*a*)] through the η-cycloheptatrienyl rings which face each other may also be significant.

The magnetic data for compounds **1**–**5** have been analysed by

Table 5 Magnetic susceptibility data for compounds **1**–**5**

Compound	Field/T	R_A[a]/K	R_B[b]/K	C/emu K mol^{-1}	θ/K	μ_{eff}/μ_B	$T(\chi_{max})$[c]/K	g[d]
1	0.2	2–300	50–300	0.29	−4.6	1.54	16	1.77
	1.0	2–300	50–300	0.29	−5.2	1.53	16	1.77
2	0.2	6–230	45–230	0.26	−2.6	1.43	12	1.65
	1.0	6–200	45–200	0.26	−4.5	1.43	12	1.65
3	0.2	6–296	—	—	—	1.44	17	1.66
4	0.2	6–296	—	—	—	1.50	13	1.73
	1.0	6–296	—	—	—	1.46	13	1.69
5	0.2	6–140	45–140	0.20	−3.6	1.27	13	1.46
	1.0	6–95	45–95	0.19	−4.2	1.23	13	1.42

[a] Temperature range within which the data were collected. [b] Temperature range within which the compound obeys the Curie–Weiss law. [c] Temperature at χ_{max}. [d] Calculated from μ_{eff} by the spin-only formula.

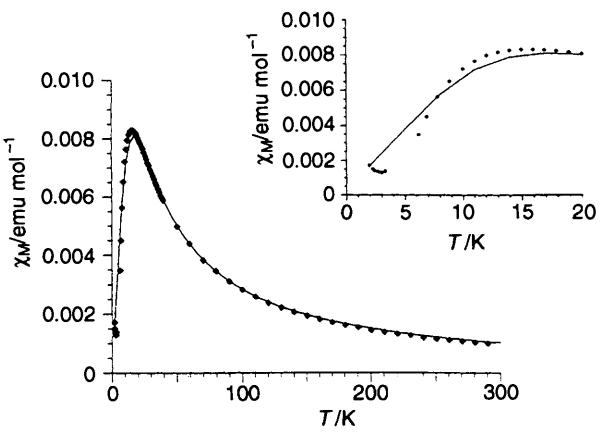

Fig. 4 Magnetic susceptibility data for [Mo(η-C_7H_7)(MeCN)I_2] **1** at 1 T. The solid line is the best fit generated by equation (2) for the one-dimensional Heisenberg model. The inset shows an expansion of the low-temperature region

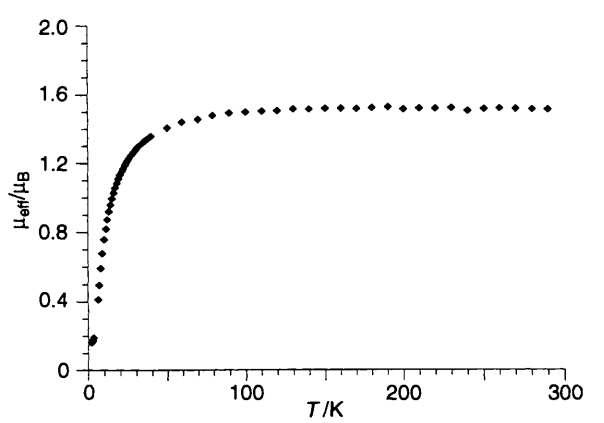

Fig. 5 Temperature variation of the effective magnetic moment for [Mo(η-C_7H_7)(MeCN)I_2] **1** at 1 T

curve-fitting using different magnetic models. Attempts to fit the data by the Bleaney–Bowers expression,[5] which assumes exchange to be significant only within a dimer, were not successful. However, close fits were obtained by using the modified Bleaney–Bowers equation[5] for an exchange-coupled pair of $S = \frac{1}{2}$ ions [equation (1)]. The term θ was included to

$$\chi_M = \left[\frac{Ng^2\mu_B{}^2}{3K(T-\theta)}\right]\left[1 + \left(\frac{1}{3}\right)\exp\left(\frac{-2J}{kT}\right)\right]^{-1} \quad (1)$$

account for interactions between the dimers. However, the best fits of equation (1) to the data yielded values of $|\theta| > |J|$ which were not acceptable since the correction terms $|\theta|$ were greater than the primary interaction parameters $|J|$.

However, we find that the susceptibility data can be described by one-dimensional chain models. Thus good fits were obtained for compounds **1**–**5** by using the Bonner–Fisher analysis for a uniformly spaced antiferromagnetic Heisenberg linear chain of $S = \frac{1}{2}$ [equation (2)] where $x = |J|/kT$.[6] Fig. 4 shows a typical

$$\chi_M = \left(\frac{Ng^2\mu_B{}^2}{kT}\right)\cdot \left(\frac{0.25 + 0.149\,95x + 0.0300\,94x^2}{1.0 + 1.9862x + 0.688\,54x^2 + 6.0626x^3}\right) \quad (2)$$

best fit based on equation (2) for [Mo(η-C_7H_7)(MeCN)I_2] **1**. The other compounds **2**–**5** gave similar fits. The values of g and J calculated from the best least-squares fits are summarised in Table 6.

In an attempt to account for the interchain interactions, a molecular field correction term was included in equation (2) giving (3),[6b] where χ_{corr} is the corrected magnetic susceptibility,

$$\chi_{corr} = \frac{\chi_{iso}}{\left[1 - \left(\frac{2zJ'\chi_{iso}}{Ng^2\mu_B{}^2}\right)\right]} \quad (3)$$

χ_{iso} is the susceptibility of an isolated Heisenberg chain of $S = \frac{1}{2}$ ions, z is the number of nearest neighbours in adjacent chains, and J' is the interchain exchange parameter. Although excellent fits were obtained for compounds **1**–**5** with this coupled-chain model, those for **1**–**4** were not acceptable since the correction terms $|zJ'|$ were even greater than the primary interaction terms $|J|$ (Table 6).

A one-dimensional Ising model can also be used to describe the magnetic behaviour. The corresponding expression for $S = \frac{1}{2}$ is shown in equation (4) where $\chi_{\|} = (Ng_{\|}{}^2\mu_B{}^2/4kT)$-

$$\chi_M = \tfrac{1}{3}\chi_{\|} + \tfrac{2}{3}\chi_{\perp} \quad (4)$$

$\exp(J/kT)$ and $\chi_{\perp} = (Ng_{\perp}{}^2\mu_B{}^2/4J)[\tanh(J/2kT) + (J/2kT)$-$\mathrm{sech}^2(J/2kT)$. Fig. 6 shows that the calculated curve corresponds quite closely to the experimental data. The best least-squares-fit parameters for compounds **1**–**5** are given in Table 6. All the one-dimensional models give best-fit g values which agree well with the experimental values obtained from susceptibility measurements (Table 5).

Some general trends can also be observed in the data in Table 6. First, changing the metal centre from molybdenum to tungsten increases the exchange constant by 1.2–1.9 K. Since the d electrons in tungsten are more diffuse than those in

Table 6 Best-fit parameters for compounds **1–5**

	One-dimensional Heisenberg model		One-dimensional Ising model		Coupled chain model		
Compound	*g*	*J*/K	*g*	*J*/K	*g*	*J*/K	*zJ'*/K
1	1.84	−8.9	1.92	−15.6	1.72	−9.0	−12.0
2	1.67	−6.9	1.75	−12.2	1.80	−6.4	−15.2
3	1.72	−10.5	1.76	−17.5	1.79	−9.9	−15.9
4	1.73	−8.1	1.78	−13.8	1.85	−7.2	−21.8
5	1.53	−7.4	1.61	−13.4	1.54	−7.4	−1.3

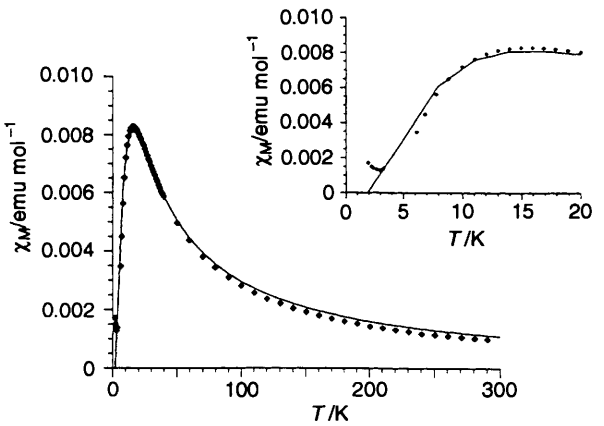

Fig. 6 Magnetic susceptibility data for $[Mo(\eta\text{-}C_7H_7)(MeCN)I_2]$ **1** at 1 T. The solid line is the best fit generated by equation (4) for the one-dimensional Ising model. The inset shows an expansion of the low-temperature region

molybdenum, it is expected that the interaction along the chain between the W–W would be stronger than for Mo–Mo. Secondly, changing the ligand from MeCN to PMe_3 decreases the *J* value by 2.0–3.7 K. It is likely that the more bulky PMe_3 ligand would lengthen the metal–metal separation in the chain resulting in smaller values for *J*. Finally, changing the halogen from iodine to bromine also decreases the value of *J* by 0.4–0.7 K. This suggests that the superexchange pathway *via* M–I–M is more efficient than for M–Br–M. In the above discussion we have assumed that compounds **2–4** are essentially isostructural with **1**. Attempts to grow single crystals of **2–4** suitable for X-ray analysis were unsuccessful.

In conclusion, we have prepared a series of 17-electron compounds $[M(\eta\text{-}C_7H_7)LX_2]$ which exhibit antiferromagnetic interaction. Model fittings suggest that the interactions are one-dimensional, which is consistent with the structure of $[Mo(\eta\text{-}C_7H_7)(MeCN)I_2]$ **1**.

Experimental

All manipulations and reactions were carried out using either standard Schlenk-line techniques under an atmosphere of dinitrogen or in an inert-atmosphere dry-box containing dinitrogen. Dinitrogen was purified by passage over a BTS catalyst and 5 Å molecular sieves. Solvents were pre-dried by standing over 5 Å molecular sieves and then distilled under an atmosphere of dinitrogen from potassium (tetrahydrofuran), sodium–potassium alloy [light petroleum (b.p. 40–60 °C)], or calcium hydride (acetonitrile). Cycloheptatriene (tech., Aldrich) was distilled before use. The compounds $MoCl_5$ and WCl_6 were used as received (Aldrich).

Infrared spectra were recorded as KBr discs on a Perkin Elmer 1510 FT-IR interferometer; mass spectra were measured by the SERC mass spectrometry service, University College, Swansea. Microanalyses were performed by the Microanalytical Department of the Inorganic Chemistry Laboratory. The EPR spectra of compounds **1** and **2** were recorded on a JEOL X-band spectrometer using 100 kHz modulation frequency and the field was calibrated using 1,1-diphenyl-2-picrylhydrazyl. The field sweep was calibrated using a standard manganese sample. The EPR spectra of compounds **3–5** were measured on a Brüker ESP 300 spectrometer.

Preparations.—$[Mo(\eta\text{-}C_7H_7)(\eta^5\text{-}C_7H_9)]$. Cold thf (400 cm^3, −20 °C) was added slowly to $MoCl_5$ (10.0 g, 36.6 mmol) which was pre-cooled at −196 °C. The mixture was allowed to warm to −78 °C then degassed cycloheptatriene (20 cm^3, 0.19 mol) was added through a cannula. The suspension turned yellow immediately. Then Na/Hg [4.2 g of Na (0.18 mol) in *ca.* 50 cm^3 of Hg] was added with stirring. The mixture was allowed to warm gradually to room temperature (r.t.) over 3 h, then it was kept stirring for 2 h at r.t. The yellow suspension became brown and then deep green during the course of the reaction. The volatiles were removed *in vacuo* and the residue was extracted with light petroleum (b.p. 40–60 °C) (4 × 75 cm^3). After filtration, the filtrate was cooled at −80 °C to give some green microcrystals which were filtered off. The filtrate was concentrated and cooled to give a second crop of green microcrystals. The combined green microcrystals were heated at 70 °C for 2 h to give the product as dark red microcrystals. Yield 4.0 g (39%).

$[Mo(\eta\text{-}C_7H_7)(MeCN)I_2]$ **1**. A solution of iodine (0.53 g, 2.1 mmol) in MeCN (30 cm^3) was added slowly to a suspension of $[Mo(\eta\text{-}C_7H_7)(\eta^5\text{-}C_7H_9)]$ (0.59 g, 2.1 mmol) in MeCN (30 cm^3). The red suspension darkened gradually during addition. The mixture was heated at 50 °C for 1 h. After filtration, the residual purple solid was extracted with MeCN (3 × 30 cm^3). The combined MeCN extract was cooled to −20 °C and dark purple microcrystals separated (0.54 g). The filtrate was concentrated to *ca.* 50 cm^3 then cooled at −20 °C again to furnish a second crop of product (0.18 g). Combined yield 0.72 g (71%).

$[Mo(\eta\text{-}C_7H_7)(PMe_3)I_2]$ **2**. The compound PMe_3 (0.1 cm^3, 1 mmol) was added to a suspension of $[Mo(\eta\text{-}C_7H_7)(MeCN)I_2]$ **1** (0.48 g, 1 mmol) in thf (80 cm^3) at r.t. The mixture was stirred for 3 h to give a red-green dichroic solution. After filtration, the filtrate was concentrated to *ca.* 30 cm^3 then cooled at −80 °C to afford the product as dark red crystals. Yield 0.41 g (79%).

$[W(\eta\text{-}C_7H_7)(\eta^5\text{-}C_7H_9)]$. Cold thf (400 cm^3, −20 °C) was added slowly to WCl_6 (12.0 g, 30.3 mmol) which was pre-cooled at −196 °C. The mixture was allowed to warm to −78 °C then degassed cycloheptatriene (16 cm^3, 0.15 mol) was added through a cannula. Sodium amalgam [4.2 g of Na (0.18 mol) in *ca.* 50 cm^3 of Hg] was added slowly with stirring, then the mixture was allowed to warm gradually to r.t. over 3 h. The mixture was kept stirring for 3 h at r.t. to give a greenish brown suspension. The volatiles were removed *in vacuo* then the residue was extracted with light petroleum (b.p. 40–60 °C) (3 × 100 cm^3). After filtration, the filtrate was concentrated to *ca.* 150 cm^3 then cooled at −80 °C to afford a brown solid. This was filtered off and the filtrate was concentrated and cooled again to give a second crop of product. Combined yield 3.0 g (27%).

$[W(\eta\text{-}C_7H_7)(MeCN)I_2]$ **3**. A solution of iodine (1.0 g, 4

Table 7 Crystal data, data collection and processing parameters for $[Mo(\eta\text{-}C_7H_7)(MeCN)I_2]$ **1**

Formula	$C_9H_{10}I_2MoN$
M	481.93
Crystal size/mm	0.20 × 0.40 × 0.50
Crystal system	Triclinic
Space group	$P\bar{1}$
a/Å	7.219(2)
b/Å	6.643(2)
c/Å	13.149(3)
α/°	96.95(2)
β/°	94.31(2)
γ/°	101.78(2)
U/Å^3	609.6
Z	2
D_c/g cm^{-3}	2.626
μ/cm^{-1}	60.26
$F(000)$	438
2θ limits/°	3–60
ω Scan width	1.00 + 0.35 tanθ
Zone	$0-h, \pm k, \pm l$
Total data collected	4183
No. of observations [$I > 3\sigma(I)$]	2606
R(merge)	0.014
No. of variables	119
Obs./variables	21.9
Weighting coefficients	51.6, −75.0, 50.1, −19.8, 5.59
Maximum/minimum peaks in final difference map/e Å^{-3}	0.79, −0.02
Root-mean-square shift/e.s.d. in final cycle	0.454
R^a	0.029
R'^b	0.033

^{a} $R = \Sigma(|F_o - F_c|)/\Sigma|F_o|$. ^{b} $R' = [\Sigma w(|F_o| - |F_c|)^2/\Sigma w|F_o|^2]^{\frac{1}{2}}$.

mmol) in MeCN (30 cm^3) was added to a suspension of $[W(\eta\text{-}C_7H_7)(\eta^5\text{-}C_7H_9)]$ (1.5 g, 4 mmol) in MeCN (30 cm^3) over 10 min. The reddish brown suspension darkened gradually during the addition. The mixture was heated at 80 °C for 3 h to give a bright red solution which was filtered and the residue was washed with MeCN (5 cm^3). The combined MeCN extract was cooled at −20 °C to give dark red microcrystals (1.5 g). These were separated and the filtrate was concentrated to *ca.* 20 cm^3 and cooled at −20 °C to furnish a second crop of product (0.5 g). Combined yield 2.0 (86%).

$[W(\eta\text{-}C_7H_7)(PMe_3)I_2]$ **4**. The compound PMe_3 (0.1 cm^3, 1 mmol) was added to a suspension of $[W(\eta\text{-}C_7H_7)(MeCN)I_2]$ **3** (0.57 g, 1 mmol) in thf (40 cm^3). The mixture was stirred at r.t. for 1 h to give a deep red solution. After filtration the filtrate was cooled at −20 °C to afford large red crystals which were filtered off and then dried *in vacuo*. The filtrate was concentrated to *ca.* 20 cm^3 and then cooled at −80 °C to give a second crop of product. Combined yield 0.42 g (70%).

$[W(\eta\text{-}C_7H_7)(PMe_3)Br_2]$ **5**. Bromine (0.13 g, 0.82 mmol) was added to a solution of $[W(\eta\text{-}C_7H_7)(\eta^5\text{-}C_7H_9)]$ (0.3 g, 0.82 mmol) in thf (20 cm^3). Precipitation occurred immediately. The suspension was stirred at r.t. for 15 min then PMe_3 (0.08 cm^3, 0.77 mmol) was added. The mixture was stirred for 1 h then filtered. The residue was washed with thf and the combined filtrate was cooled at −80 °C to give the product as orange-brown crystals. Yield 0.18 g (44%).

Crystal Structure Determination of Compound **1**.—Crystal data, data-collection and processing parameters are given in Table 7. The general procedure was as follows. A crystal was mounted in a Lindemann tube (0.7 mm) under dinitrogen and sealed with a small flame. This was transferred to the goniometer head of an Enraf-Nonius CAD4 diffractometer interfaced to a PDP 11/23 minicomputer. Unit-cell parameters were calculated from the setting angles of 25 carefully centred reflections. Three reflections were chosen as intensity standards and were measured every 3600 s of X-ray exposure time, and three orientation controls were measured every 250 reflections. The data were collected at room temperature using graphite-monochromated Mo-Kα radiation (λ = 0.710 69 Å) and an ω–2θ scan mode.

The data were corrected for Lorentz and polarisation effects and an empirical absorption correction[8] based on azimuthal scan data was applied. Equivalent reflections were merged and systematically absent reflections rejected. The locations of the molybdenum and iodine were determined from a Patterson synthesis. Subsequent Fourier-difference-syntheses revealed the positions of other non-hydrogen atoms. Non-hydrogen atoms were refined with anisotropic thermal parameters by full-matrix least-squares procedures. Hydrogen atoms were placed in estimated positions (C–H 0.96 Å) with fixed isotropic thermal parameters and refined riding on their supporting carbon atoms. A Chebyshev weighting scheme[9] was applied and the data were corrected for the effects of anomalous dispersion and isotropic extinction (*via* an overall isotropic extinction parameter[10]) in the final stages of refinement. All crystallographic calculations were performed using the CRYSTALS suite[11] on a Micro VAX 3800 computer in the Chemical Crystallography Laboratory, Oxford. Neutral atom scattering factors were taken from the usual sources.[12]

Additional material available from the Cambridge Crystallographic Data Centre comprises H-atom coordinates, thermal parameters and remaining bond lengths and angles.

Magnetic Measurements.—In an inert-atmosphere dry-box, the powdered samples of compounds **1**–**5** were loaded into quartz buckets and sealed with a cap. Magnetic data were then collected on a Cryogenics Consultants SCU 500 SQUID magnetometer in conjunction with a Lakeshore DRC-91C temperature controller. The susceptibilities have been corrected for the intrinsic diamagnetism of the sample container and the diamagnetism of the sample. The latter quantity was calculated by plotting the susceptibilities measured from 130 K onward [or for compound **5** between 70 and 95 K (0.2 T) or 90 and 140 K (1 T)] against $1/T$, and reading the intercept on the susceptibility axis.

Acknowledgements

We thank Dr. A. R. Chaudhuri for assistance in magnetic susceptibility measurements, Patrick C. McGowan for collecting the X-ray data, and the Croucher Foundation of Hong Kong for a scholarship (to D. K. P. N.).

References

1 L. J. de Jough and A. R. Miedema, *Adv. Phys.*, 1974, **23**, 1; *Magneto-Structural Correlations in Exchange Coupled Systems*, eds. R. D. Willett, D. Gatteschi and O. Kahn, D. Reidel, Dordrecht, 1985; *Extended Linear Chain Complexes*, ed. J. S. Miller, Plenum, New York, 1981–1983, vols. 1–3.

2 (*a*) M. L. H. Green, D. K. P. Ng and R. C. Tovey, *J. Chem. Soc., Chem. Commun.*, 1992, 918; (*b*) M. L. H. Green and D. K. P. Ng, *J. Chem. Soc., Chem. Commun.*, 1992, 1116.

3 E. M. van Dam, W. N. Brend, M. P. Silvon and P. S. Skell, *J. Am. Chem. Soc.*, 1975, **97**, 465.

4 C. E. Davies, I. M. Gardiner, J. C. Green, M. L. H. Green, N. J. Hazel, P. D. Grebenik, V. S. B. Mtetwa and K. Prout, *J. Chem. Soc., Dalton Trans.*, 1985, 669; J. C. Green, M. L. H. Green, N. Kaltsoyannis, P. Mountford, P. Scott and S. J. Simpson, *Organometallics*, 1992, **11**, 3353.

5 R. L. Carlin, *Magnetochemistry*, Springer, Berlin, 1986, ch. 5.

6 (*a*) J. C. Bonner and M. E. Fisher, *Phys. Rev., A*, 1964, **135**, 640; (*b*) W. E. Hatfield, R. R. Weller and J. W. Hall, *Inorg. Chem.*, 1980, **19**, 3825.

7 M. E. Fisher, *J. Math. Phys.*, 1963, **4**, 124; A. Pires and D. Hone, *J. Phys. Soc. Jpn.*, 1978, **44**, 43.

8 A. C. T. North, D. C. Philips and F. S. Mathews, *Acta Crystallogr., Sect. A*, 1968, **24**, 351.
9 J. S. Rollet, *Computing Methods in Crystallography*, Pergamon, Oxford, 1985.
10 A. C. Larson, *Acta Crystallogr., Sect. A*, 1967, **23**, 664.
11 D. J. Watkin, J. R. Carruthers and P. W. Betteridge, *CRYSTALS User Guide*, Chemical Crystallography Laboratory, University of Oxford, 1985.
12 *International Tables for X-Ray Crystallography*, Kynoch Press, Birmingham, 1974, vol. 4.

Received 19*th January* 1993; *Paper* 3/00336A